Systems/Circuits

Dorsolateral Striatum is a Bottleneck for Responding to Task-Relevant Stimuli in a Learned Whisker Detection Task in Mice

Behzad Zareian,[1*] Angelina Lam,[2*] and Edward Zagha[1,2,3]

[1]Department of Psychology, University of California Riverside, Riverside, California 92521, [2]Division of Biomedical Sciences, School of Medicine, University of California Riverside, Riverside, California 92521, and [3]Neuroscience Graduate Program, University of California Riverside, Riverside, California 92521

A learned sensory-motor behavior engages multiple brain regions, including the neocortex and the basal ganglia. How a target stimulus is detected by these regions and converted to a motor response remains poorly understood. Here, we performed electrophysiological recordings and pharmacological inactivations of whisker motor cortex and dorsolateral striatum to determine the representations within, and functions of, each region during performance in a selective whisker detection task in male and female mice. From the recording experiments, we observed robust, lateralized sensory responses in both structures. We also observed bilateral choice probability and preresponse activity in both structures, with these features emerging earlier in whisker motor cortex than dorsolateral striatum. These findings establish both whisker motor cortex and dorsolateral striatum as potential contributors to the sensory-to-motor (sensorimotor) transformation. We performed pharmacological inactivation studies to determine the necessity of these brain regions for this task. We found that suppressing the dorsolateral striatum severely disrupts responding to task-relevant stimuli, without disrupting the ability to respond, whereas suppressing whisker motor cortex resulted in more subtle changes in sensory detection and response criterion. Together these data support the dorsolateral striatum as an essential node in the sensorimotor transformation of this whisker detection task.

Key words: **inactivation; neocortex; response criterion; sensorimotor transformation; sensory detection; striatum**

Significance Statement

Selecting an item in a grocery store, hailing a cab – these daily practices require us to transform sensory stimuli into motor responses. Many decades of previous research have studied goal-directed sensory-to-motor transformations within various brain structures, including the neocortex and the basal ganglia. Yet, our understanding of how these regions coordinate to perform sensory-to-motor transformations is limited because these brain structures are often studied by different researchers and through different behavioral tasks. Here, we record and perturb specific regions of the neocortex and the basal ganglia and compare their contributions during performance of a goal-directed somatosensory detection task. We find notable differences in the activities and functions of these regions, which suggests specific contributions to the sensory-to-motor transformation process.

Introduction

Goal-directed behavior requires the ability to selectively detect and respond to target sensory stimuli, while inhibiting responses to extraneous or distractor stimuli. In simple Go/NoGo tasks, sensory selection involves transforming sensory responses into motor commands. Neuronal recording studies have demonstrated full sensory-to-motor (sensorimotor) transformations unfolding across the neocortex, with motor planning and motor command signals present most robustly in motor cortices (Moran and Desimone, 1985; Hanes and Schall, 1996; Salinas and Romo, 1998; de Lafuente and Romo, 2006; Li et al., 2015, 2016; Siegel et al., 2015; Inagaki et al., 2019; Esmaeili et al., 2021; Finkelstein et al., 2021). These studies

Received Aug. 5, 2022; revised Feb. 1, 2023; accepted Feb. 3, 2023.

Author contributions: B.Z. and E.Z. designed research; B.Z. and A.L. performed research; B.Z., A.L., and E.Z. analyzed data; B.Z. wrote the first draft of the paper; B.Z., A.L., and E.Z. edited the paper; B.Z., A.L., and E.Z. wrote the paper.

This work was support by the National Institutes of Health Grant R01NS107599 (to E.Z.). We thank Trevor Zimmerman-Thompson and Emaan Kaur for helping with training of mice. We also thank Zhaoran Zhang, Krista Marrero, and Krithiga Aruljothi for their feedback in all stages of the project.

*B.Z. and A.L. contributed equally to this work.

The authors declare no competing financial interests.

Correspondence should be addressed to Edward Zagha at edward.zagha@ucr.edu.

https://doi.org/10.1523/JNEUROSCI.1506-22.2023

provided strong motivation for considering the neocortex as the primary structure implementing goal-directed, sensorimotor transformations. Simultaneously, anatomical, physiological, and lesioning studies of the basal ganglia identified these subcortical structures as essential for implementing action selection and initiation (Alexander and Crutcher, 1990; Graybiel et al., 1994; Yin et al., 2004; Grillner et al., 2005; Jin and Costa, 2010; Stephenson-Jones et al., 2011; Bergstrom et al., 2018, 2020). Motor cortex and dorsolateral striatum are heavily interconnected, as determined by both anatomical and functional studies (McGeorge and Faull, 1987; Frank et al., 2001; Saunders et al., 2015; Hintiryan et al., 2016; Hunnicutt et al., 2016; Kupferschmidt et al., 2017; C.R. Lee et al., 2019; Foster et al., 2021; Peters et al., 2021; Gordon et al., 2022), and therefore sensorimotor transformations may be mediated by the coordinated activities of both regions. Traditional models of cortico-striatal coordination propose that motor plans are generated in motor cortex and then selected in the basal ganglia. The output of this striatal selection is propagated via the thalamus back to motor cortex, which ultimately sends out the motor command (Hoover and Strick, 1999; Redgrave et al., 1999; Middleton and Strick, 2000). And yet, the basal ganglia project to multiple regions besides the neocortex which may also trigger motor commands (Mink, 1996; Yin and Knowlton, 2006; Utter and Basso, 2008; Guo et al., 2017). Revealing the functional organizations of the motor cortex and the basal ganglia requires conducting representational and causal studies from both structures in subjects performing the same behavioral task (Pasupathy and Miller, 2005; Muhammad et al., 2006; Clarke et al., 2008; Antzoulatos and Miller, 2011; Kupferschmidt et al., 2017; Peters et al., 2021; Brockett et al., 2022; Pimentel-Farfan et al., 2022).

The mouse whisker system is an ideal model system to test this functional organization, because of its simplified and well-characterized neural anatomy. Whisker stimulus responses propagate to the contralateral whisker representation of primary somatosensory cortex (S1). In turn, S1 projects directly and robustly to subregions of both the whisker motor cortex (wMC) and the dorsolateral striatum (DLS) (Mao et al., 2011). This study focuses on these subregions of wMC and DLS, as possible signaling pathways for sensorimotor transformations. In comparing wMC and DLS contributions to task performance, we propose two extreme models in which one region is a "bottleneck" (Fig. 1*C*,*D*), by which we mean, an indispensable node along the sensorimotor transformation signaling pathway. A brain region may be indispensable but not a signaling bottleneck – for example, a region that is a general regulator of arousal, motivation, or movement initiation. To identify a bottleneck, we implement two criteria. First, recording studies must identify task-specific sensory, motor, and/or choice-related activities. Second, causal studies must demonstrate severe impairments in task performance that are not accounted for by global changes in arousal, motivation, or movement.

Prior representational and causal studies implicate the involvement of both wMC and DLS in whisker detection/discrimination tasks (Guo et al., 2014; Li et al., 2015, 2016; Sippy et al., 2015; Zagha et al., 2015; Hong et al., 2018; C.R. Lee et al., 2019; Aruljothi et al., 2020; Zareian et al., 2021). And yet, the functional organizations between these regions in the context of whisker sensorimotor transformations remains poorly understood. In this study, we directly compared the representational and functional properties of wMC and DLS in a Go/NoGo selective whisker detection task (Fig. 1). We previously demonstrated robust sensory, motor, and choice signals in wMC, identifying this region as the most likely site of sensorimotor transformations within dorsal neocortex for this task (Aruljothi et al., 2020; Zareian et al., 2021). In the current study, our data support a functional organization in which DLS an essential bottleneck for transforming whisker stimuli into motor commands, with modulatory contributions from wMC to sensory detection and response criterion.

Materials and Methods

Animals

Experiments performed in this study were approved by the Institutional Animal Care and Use Committee of University of California, Riverside. Male and female mice of two strains were used for the experiments: wild-type (C57BL/6J) and Thy1-ChR2 mice (all purchased from The Jackson Laboratory or bred in our own colony). Data from mice of each sex and strain were combined, and the transgenic feature was not exploited in these studies. All mice were housed on a 12/12 h light/dark cycle. Food was always accessible to mice outside of the behavioral training sessions.

Surgery

All experiments were performed on head-fixed mice. To attach the headpost to the skull, the mice were first anesthetized with a mixture of ketamine (100 mg/kg), xylazine (10 mg/kg), and isoflurane (1–2%) throughout the surgery. They were additionally administered meloxicam (5 mg/kg) and enrofloxacin (5 mg/kg) at the day of the surgery and for 2 d postsurgery. A 10 mm × 10 mm part of scalp was resected. A stainless steel headpost with length of 3 cm and a weight of 1.5 g with a central window of 8 × 8 mm, was attached to the skull using cyanoacrylate glue. The 8 × 8-mm exposed window was sealed with Kwik-sil. After the surgery, the mice recovered on a heating pad. Behavioral experiments were started a minimum of 3 d after recovery from surgery. At the day of recording or inactivation, small craniotomies (~0.5 mm diameter) were made under isoflurane anesthesia to access the relevant cortical and subcortical regions (see below).

Training

We trained mice in a selective whisker detection task, which we have characterized in previous studies (Aruljothi et al., 2020; Zareian et al., 2021; Marrero et al., 2022). The mice were head-fixed in a custom-made setup. Piezo-controlled paddles were placed symmetrically within bilateral whisker fields contacting multiple whiskers. Target and distractor whisker fields were assigned at the beginning of training (target as the right whisker field) and remained constant throughout. Sensory stimuli consisted of small, rapid deflections of either whisker field. The deflections ranged from 0.01 to 0.2 s in duration with a velocity of 10 mm/s, always equal for target and distractor stimuli. For most of the training sessions, two different stimulus amplitudes were used, one (large) near the saturation of the mouse's psychometric range and the other (small) near the midpoint. Mice reported stimulus detection by licking a central lick port. A lockout of 0.2 s was imposed between stimulus onset and response window, and mice were punished with a timeout for responding during this delay. Following 5- to 9-s intertrial intervals, mice received either target, distractor, or catch (no stimulus) trials. All licking outside the post-target response window were punished by time out (resetting the intertrial interval). Water rewards for responding during the post-target response window were delivered from the same lick port used to report stimulus detection. Mice were water restricted throughout the training period, with the goal of receiving all water during behavioral trainings. Supplemental water was given in the home cage if weights fell below 85% of initial weights. Behavioral training was implemented using custom MATLAB scripts and Arduino Uno boards to trigger task stimuli and report licking responses. For further details of the behavioral training and training stages, see Aruljothi et al. (2020).

Mice were considered expert in the task once they achieved a target-distractor discrimination d-prime > 1, for three consecutive days [d-prime=*norminv* (Hit rate)- *norminv* (False alarm rate), in which *norminv* is the inverse of the standard normal cumulative distribution value]. All recording and inactivation experiments were performed in animals that

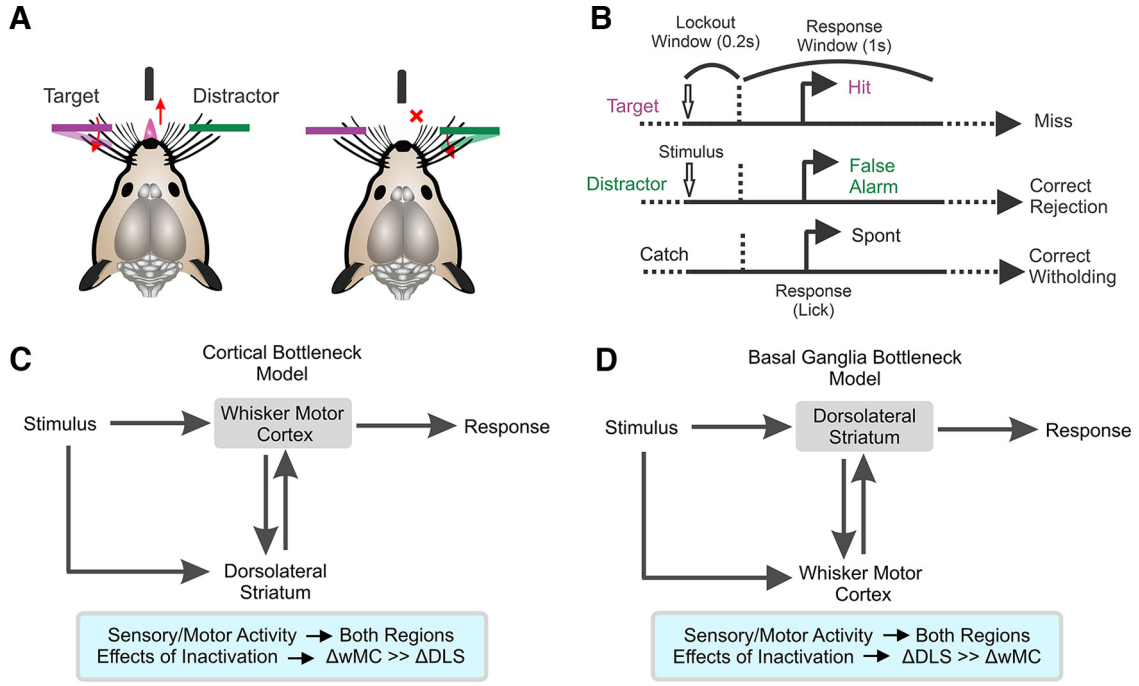

Figure 1. Behavioral task, trial structure, and possible functional organizations underlying sensorimotor transformations. ***A***, Illustration of the behavioral task. Mice learn to respond (lick) to small, transient whisker deflections in one of their whisker fields (purple, target) and to withhold licking to identical deflections in their opposite whisker field (green, distractor; modified from Aruljothi et al., 2020). ***B***, Diagram of task structure for the operant, selective detection task (also see Materials and Methods). Following a variable (5–9 s) intertrial interval, mice receive either a target stimulus, distractor stimulus, or catch trial. After stimulus onset, a lockout window of 0.2 s is implemented in which responding is punished by immediately restarting the intertrial. Responses during the response window of target trials are considered hits and responses during the response window of distractor trials are considered false alarms. ***C***, ***D***, Different models (top) and their experimental predictions (bottom) for the pathways involved in converting whisker stimuli into motor responses. The models differ in the involvement and importance of sensory-to-motor transformations through the whisker motor cortex versus the dorsolateral striatum.

had reached expert performance. For the electrophysiological recording sessions, performance values (discrimination d-prime) were as follows: target-aligned wMC: 2.7 ± 0.6, $n = 11$, distractor-aligned wMC: 2.5 ± 0.6, $n = 19$, target-aligned DLS: 2.3 ± 0.6, $n = 10$, distractor-aligned DLS: 2.3 ± 0.7, $n = 11$ (mean ± SD). Performance of the mice during muscimol inactivation are reported in the Results, since behavioral performance was the dependent variable under examination.

Electrophysiological recordings

A total of 16 mice were used for electrophysiological recording experiments (see Table 1 for the number of sessions used in each analysis). Recordings were conducted following at least 20 min after recovery from isoflurane anesthesia. Recovery was assessed based on normal mouse behavior within their home cage and high engagement during the first few minutes of the task. For wMC and DLS recordings, Neuronexus laminar probes with 16 sites and 100-µm spacing were used (A1x16-5 mm-100-177-OA16LP or A1x16-5 mm-100-177-A16). For each recording, the probe was advanced slowly in the brain using hydraulic Narishige micromanipulators. Electrophysiology data were acquired using Neuralynx recording system and Cheetah viewer software. The data were acquired at 32 kHz, then subsequently filtered at 600–6000 Hz for spike analyses.

Craniotomies for wMC recordings were centered on 1 ± 0.5 mm lateral, 1 ± 0.5 mm anterior to bregma. These wMC coordinates were chosen to target the S1 projection zone, as in our previous studies (Zareian et al., 2021). The probe was advanced until the last site was partially visible at the surface (16 sites spanning 1.5 mm within cortex and below). At these coordinates, layers 1, 2/3 and 5A of wMC collectively span the superficial (dorsal) 500–600 µm (Hooks et al., 2013; also see Fig. 2*C*). Therefore, we considered recording sites within this range as "superficial wMC" and the more ventral recording sites as "deep wMC." DLS coordinates were as follows (from bregma): 2.5 ± 0.5 mm lateral, 0.7 ± 0.4 mm posterior (also see Fig. 2*G*). The probe was advanced deep inside the DLS (distal tip 2300–2500 µm below the pial surface). The coordinates were initially chosen based on Allen Brain Institute Mouse Connectivity atlas, Allen Institute for Brain Science (2004) selecting the region within DLS receiving the highest density inputs from S1. We recorded 3.2 ± 1.2 sessions per mouse (mean ± SD). In three of the 16 mice, we recorded from both wMC and DLS, although during separate behavioral sessions. Only one session was recorded per mouse per day.

Table 1. Session numbers (*N*) used for electrophysiological recordings

Session *N*s					
Electrophysiological experiments	Figure 3	Figure 4, hits	Figure 4, FAs	Figure 5	Figure 6
twMC	11	11	7	11	7
tDLS	10	10	9	10	8
dwMC	Not used	19	17	19	6
dDLS	Not used	11	10	11	8
Total sessions	21	51	43	51	29

The number of sessions for each region used for analyses in different figures, related to recording experiments.

Muscimol inactivation

Injections of 2 mM muscimol in normal saline were performed using the Nanoject III Programmable Nanoliter Injector from Drummond Scientific Company fitted with a borosilicate glass micropipette. The same surface coordinates were used for muscimol injections as described above for electrophysiological recordings. For wMC injections, 250 nl of muscimol was injected at a rate of 1–3 nl/s at 1 mm deep (from the pial surface) and another 250 nl was administered at 0.5 mm deep, for a total of 500 nl, to target both superficial and deep layers of wMC. Based on previous experience using nearly identical protocols, this application causes inactivation of cortex ~1 mm in diameter as observed from the dorsal surface (see Salkoff et al., 2020; their Figure 4D, and histologic verification described below). For DLS injections, a single bolus of 250 nl of 2 mM muscimol was injected at a rate of 1–3 nl/s at 1.7 mm deep.

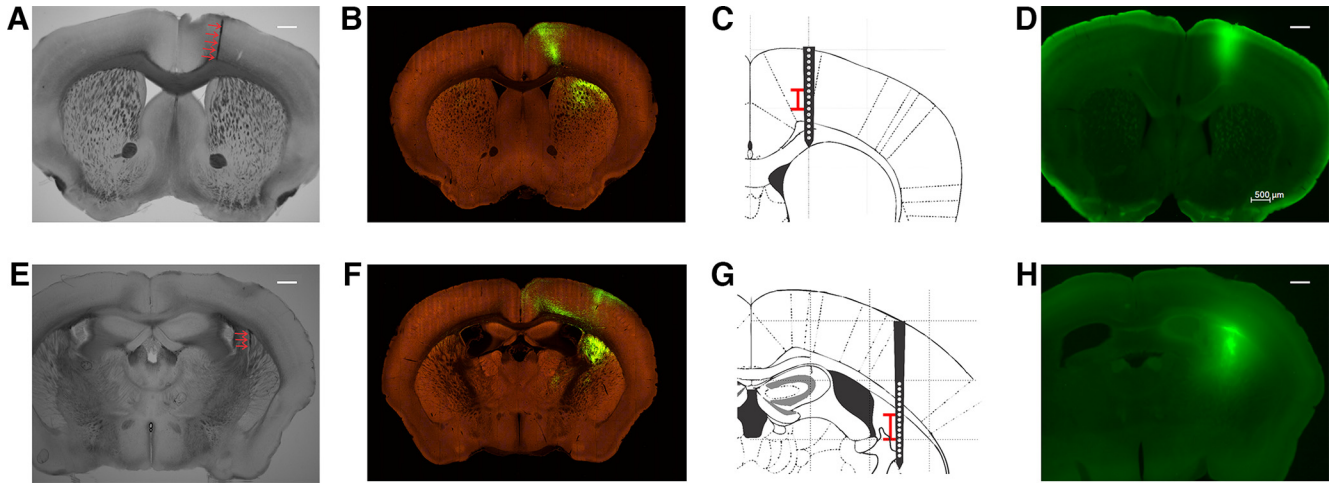

Figure 2. wMC and DLS subregion targeting. ***A***, ***E***, Coronal brain sections from individual mice depicting the needle tracts (red arrows) from targeting wMC (***A***) and DLS (***E***). ***B***, ***F***, Findings from whisker-related S1 axonal labeling from the Allen Mouse Brain Connectivity Atlas, https://connectivity.brain-map.org/projection/experiment/126907302, showing the S1-projection sites (green) in wMC (***B***, section 49) and DLS (***F***, section 62). ***C***, ***G***, Schematics of the same coronal sections as in ***A***, ***B*** and ***E***, ***F***, respectively, illustrating the coverage of the laminar multisite electrode recordings (data were compiled from target-aligned and distractor-aligned recordings, projected onto the same hemisphere). Red bars indicate the mean ± 1 SD for the sites with maximum sensory encoding within each region. ***D***, ***H***, Coronal brain sections depicting spread of fluorescent muscimol in wMC (***D***) and DLS (***H***). For panels ***A***, ***D***, ***E***, ***H***, the scale bars are 0.5 mm and the histological images are representative data from individual mice.

For muscimol inactivation studies, expertly performing mice were assigned to alternating control performance days without muscimol exposure and experimental performance days with muscimol inactivation. Sites for muscimol inactivation were randomized for each mouse, such that the order of inactivation varied (both within and across mice). Only one region was inactivated per day, with interleaved noninactivated control days. The average number of regions inactivated for each mouse was 2.6 ± 1.2 regions per mouse (mean ± SD). All four regions were inactivated in 2 of the 7 mice used in these experiments. For each mouse, the range of inactivations for a single region varied from 0–3. For daily behavioral testing, mice were first placed in a classical conditioning version of our task (see Aruljothi et al., 2020) for 2 min to ensure licking responses were intact when presented with water reward cued by the opening of a solenoid. Subsequently, mice were tested in the full selective detection task for 1 h. After 1 h of testing if mice collected fewer than 10 rewards, they were considered nonperformers. 10 rewards was selected as the performance criterion since it is 2–3 SDs below the number of rewards achieved by noninjected control mice within the same duration [62 ± 21 rewards (mean ± SD)]. Nonperforming mice were placed back in the classical conditioning task for 15 min to again assess for licking to solenoid-cued water rewards. If mice were still performing the full selective detection task after 1 h, they were permitted to perform that task until unmotivated (as determined by time since previous reward >10 min). The threshold for consideration as "performing" in the classical conditioning task was responding to >50% of rewards, in either testing phase.

Histology

Verifications of silicon probe and muscimol injection sites and quantification of muscimol spread were performed on wild-type C57BL/6J mice not previously used for muscimol inactivation experiments. A borosilicate glass micropipette was inserted into wMC or DLS using similar protocols as for muscimol inactivation studies. To quantify the spatial extent of muscimol inactivation, a fluorescent conjugated muscimol was used (Muscimol, BODIPY TMR-X Conjugate, Invitrogen, lot #2403710), dissolved in a 5% v/v of DMSO in normal saline to reach a final concentration of 2 mM, with the same injection protocols and volumes as described above. One hour after injection, mice brains were processed to visualize the pipette tract and/or fluorescence spread. Mice were sacrificed using Euthasol euthanasia solution and transcardially perfused with 20–40 ml of 1× PBS solution followed by 20–40 ml of 4% paraformaldehyde (PFA) in 1× PBS before the brains were was dissected and stored in 4% PFA overnight. The following day, brains were rinsed with 1× PBS three times, then embedded in a 3% agarose in 1× PBS solution; 120 μm slices were collected using a Leica VT1000 S vibrating blade microtome and mounted onto glass slides using glycerol and a coverslip. 2× images were collected using a Keyence BZ-X710. Quantification of fluorescent muscimol spread was performed using ImageJ to calculate the full width at half maximum (FWHM). For individual injections, FWHM values were calculated as: wMC ($n = 2$ mice), 480 and 560 µm; DLS ($n = 3$ mice), 630, 650, and 790 µm.

Comparison tracing studies (Fig. 2*B*,*F*) are from the Allen Brain Mouse Connectivity Atlas, experiment 126907302 (Oh et al., 2014). For the schematics depicting approximate recording sites (Fig. 2*C*,*G*), we traced the outlines of slices from The Mouse Brain in Stereotaxic Coordinates (−1.06 and 0.98 mm from bregma for DLS and wMC, respectively; Paxinos and Franklin, 2019). We compared the cortical thickness from the atlas to our functional estimates based on white matter location and determined a scale factor of 17%. Accordingly, a 17% reduction was applied to the mapping of the recording sites onto the atlas schematics.

Quantification and statistical analysis

Analyses were performed using custom MATLAB scripts or SPSS and displayed using Corel Draw. For all statistical analyses, we used $\alpha = 0.05$ as significance threshold, unless otherwise stated. Data are presented as mean ± SEM, unless otherwise stated. Analyses focused on large amplitude target and distractor stimuli.

Multiunit activity (MUA) analyses

Combined behavioral-recording sessions were truncated to include a single engaged period (a continuous bout of at least 10 min of task performance with no gaps in responding (licking) >60 s). MUA was identified as negative-going threshold crossings over 3× SD of the bandpass filtered voltage fluctuations throughout that session (Figs. 3-6). For wMC recordings, electrode channels 1–7 (spanning the superficial 600 µm) were considered as superficial layers. The remaining channels (8–16) were considered as deep layers. For DLS data analyses, we first determined the location of the white matter, as the site within the middle 5–12 sites with the minimum average spiking. The recording sites below that were considered as putative DLS sites.

Spike counts were binned in 5 ms bins throughout each recording session and combined as needed for larger window analyses. We calculated sensory detection and choice probability values using signal detection theory (Zareian et al., 2021). Briefly, the sensory detection was calculated by considering the area under the receiver operating

characteristic (ROC) curve constructed from plotting cumulative distributions of spiking of a poststimulus window against prestimulus baseline activity. For baseline activity, three consecutive epochs with the same size as the poststimulus window were considered. Poststimulus window sizes were either 5 ms bins for continuous d-prime traces (Fig. 4*A–D*) or a single 100-ms window immediately poststimulus (Fig. 4*E*,*F*). For latency to reaction time analyses (Fig. 5), a window of 1 s before the reaction time was considered as baseline.

Similarly, choice probability was calculated as the area under the ROC curve constructed from plotting the cumulative distributions of spiking activity on hit trials against miss trials. The choice probability traces were calculated from 50-ms sliding windows with 90% overlap. For statistical comparisons, the session choice probability values were compared with chance level (50%). For choice probability analysis and comparing temporal differences of hit and miss trials (Fig. 6*G*), sufficient hit and miss trials were assessed based on previously described criteria (Zareian et al., 2021). Choice probability latency was determined as the time from stimulus onset to rise above 60% choice probability.

Muscimol inactivation analyses

For the muscimol inactivation experiments, we obtained task engagement time, hit rate, false alarm rate, catch rate, d-prime, and criterion using a 1-h time window of selective detection task performance (Figs. 7-9). Data were averaged across all sessions and all mice for each set of analyses (from $n = 7$ total mice, see Table 2 for the number of sessions used). Task engagement times (Fig. 7*E*) were calculated as the sum of all times mice were active during the task, as defined by no lapse in licking >1 min. For Figure 9*B* d-prime and criterion calculations are detection measures based on hit rate and catch rate, unlike discrimination measures based on hit rate and false alarm rate as reported in Figure 8. The Δ d-prime (criterion) for target stimulus detection was calculated as the difference between the average detection d-prime (criterion) for inactivation sessions and the average detection d-prime (criterion) for noninjected control sessions. For Figure 9*C*, the averaged modulation index for each inactivation group was calculated as the difference between hit rates and catch rates divided by the sum of hit rates and catch rates for each session. Four inactivation sessions were excluded from this analysis (one twMC, three tDLS) because of hit rates and catch rates of 0% (see Table 2 for summary data).

Statistical analyses

For statistical comparisons of recording experiments, *t* test or ANOVA were used. ANOVA statistics were calculated using either SPSS or MATLAB. We considered region and hemisphere effects by running two-way ANOVA tests; performance measures were grouped regionally (main effect of wMC vs DLS regions regardless of the hemisphere) and grouped by hemisphere (main effect of target-aligned vs distractor-aligned regions regardless of brain regions). "Target-aligned" or "distractor-aligned" refers to the hemisphere contralateral to the whisker field that receives target or distractor paddle deflections, respectively. Interaction effects were also considered (regional × hemisphere). For pairwise comparisons, Tukey–Kramer *post hoc* multiple comparison test using *multcompare* function in MATLAB were conducted between pairs of conditions (twMC, tDLS, dwMC, dDLS). For muscimol inactivation studies, we additionally compared overall performance rates using χ^2 tests and compared inactivation sessions to noninjected control sessions using unpaired *t* tests.

Results

Behavioral task, model predictions, and regions of interest

We trained mice in a head-fixed, whisker-based selective detection task (Aruljothi et al., 2020; Zareian et al., 2021; Marrero et al., 2022). In this task, mice learned to respond (lick) to small, transient whisker deflections within one whisker field (target) and to ignore identical whisker deflections in the opposite whisker field (distractor) (Fig. 1*A*). Because of the lateralization of the somatosensory system, this task configuration establishes "target-aligned" and "distractor-aligned" cortical and striatal fields that are symmetric across midline and contralateral to the deflected whiskers. In the task structure, we impose a 200-ms lockout between stimulus onset and response window, and mice learn to withhold responding across this delay (Fig. 1*B*). Mice are considered expert in this task once they achieve a separation (d-prime) between hit rate (response to target) and false alarm rate (response to distractor), >1, for three consecutive days (for training details, see Materials and Methods and Aruljothi et al., 2020).

Table 2. Session numbers (*N*) used for muscimol inactivation experiments

Session *N*s		
Inactivation experiment type	Figures 7, 8, 9*A*,*B*	Figure 9*C*
Control	72	72
twMC	12	11
tDLS	10	7
dwMC	13	13
dDLS	10	10
Total sessions	117	113

The number of sessions for each region used for analyses in different figures, related to control and inactivation experiments.

Electrophysiological recording and muscimol inactivation studies were conducted in expert mice, while they were performing the selective detection task. These physiological studies focused on two major outputs of primary somatosensory cortex (S1): the S1-projection subregions of both the whisker motor cortex (wMC) and the dorsolateral striatum (DLS) (Mao et al., 2011).

We recognize two general functional organizations of these S1-output pathways (Fig. 1*C*,*D*), in which either wMC or DLS functions as the primary node for transforming whisker stimuli into licking responses. From the cortical bottleneck model (Fig. 1*C*), we would expect robust sensory and motor activities in both wMC and DLS, yet inactivating wMC to have the larger effects on task performance. From the basal ganglia bottleneck model (Fig. 1*D*), we would expect robust sensory and motor activities in both regions, yet inactivating DLS to have the larger effects on task performance. Subsequent experiments and analyses were designed to distinguish between these models.

Robust sensory-related and motor-related spiking activities in wMC and DLS

Figure 2 depicts examples of wMC and DLS targeting for our recording and perturbation experiments, relative to S1 axonal projections. We performed laminar electrophysiological recordings and compared the multiunit activity (MUA) signals from wMC and DLS. For each recording session, we identified the site with the largest sensory encoding (neurometric d-prime; see Materials and Methods for details) and used the activity at that site for all subsequent analyses. For wMC, the laminar electrode spanned all layers, and sensory encoding was invariable largest in deep layers (1023 ± 37 μm, $n = 30$ sessions, $n = 11$ sessions in target-aligned wMC and $n = 19$ sessions in distractor-aligned wMC; Fig. 2*C*). For DLS, sensory encoding was largest 2136 ± 55 μm from the cortical surface and 452 ± 53 μm below the putative white matter ($n = 21$ sessions, $n = 10$ sessions in target-aligned DLS and $n = 11$ sessions in distractor-aligned DLS; Fig. 2*G*).

In Figure 3, we display poststimulus and preresponse spiking activities for target stimuli in target-aligned wMC (twMC) and in target-aligned DLS (tDLS). In both regions, MUA appeared at short latency after stimulus onset (Fig. 3*A*,*B*, left columns). We consider this activity to be "sensory" because it occurs regardless

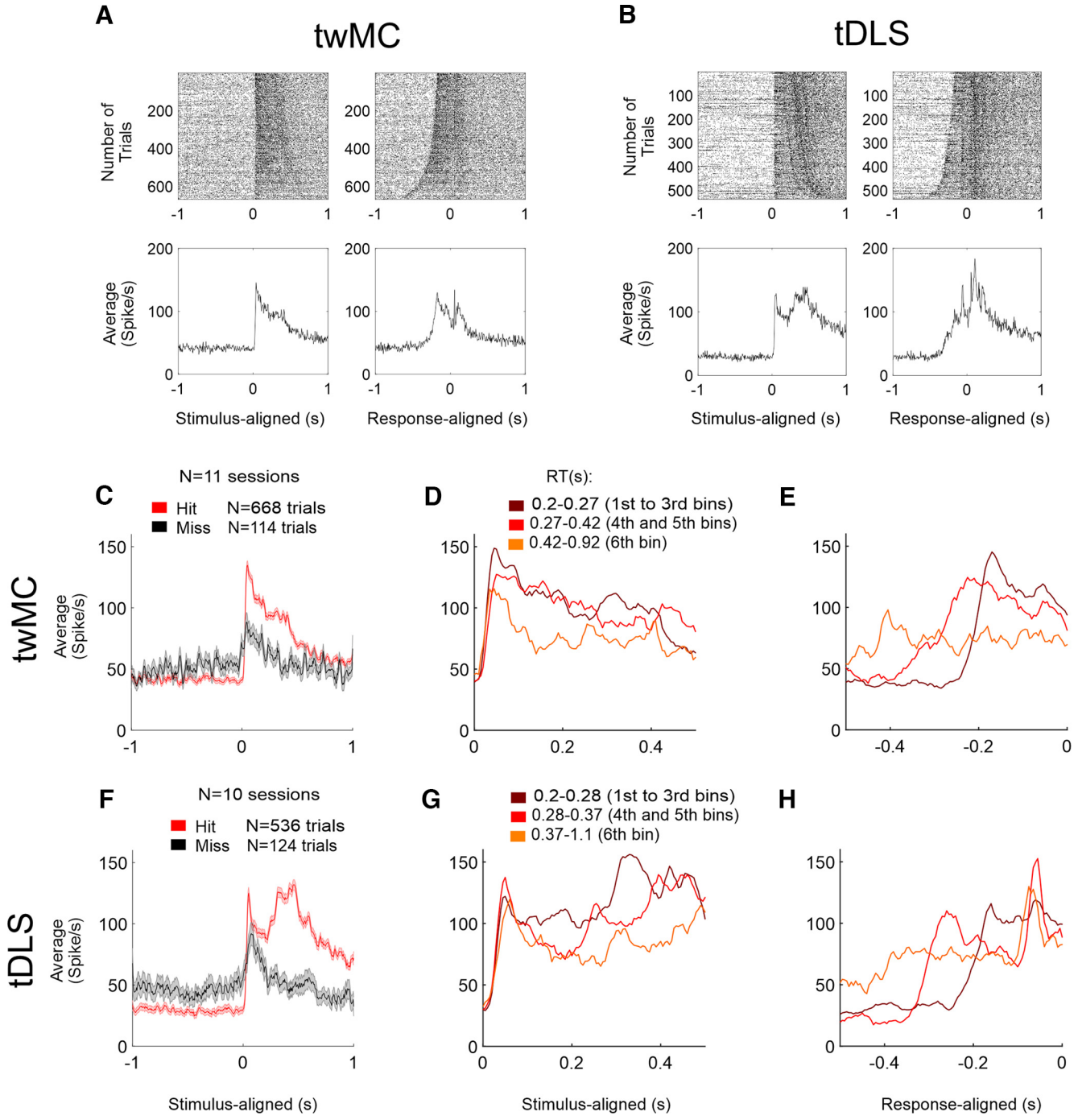

Figure 3. Robust poststimulus and preresponse spiking activities in target-aligned wMC and DLS. ***A***, MUA recorded from deep layers of target-aligned wMC for all hit trials, pooled across sessions. The left column depicts MUA aligned to the target stimulus onset and the right column depicts MUA aligned to the reaction time. Top panels show raster plots sorted based on reaction times from fast (top) to slow (bottom) hits trials. Bottom panels show average of all trials shown in the top panels. Note the rapid poststimulus (left, putative sensory) and the robust preresponse (right, putative motor) spiking activities. ***B***, Same as ***A*** but recorded from target-aligned DLS. ***C***, Average of all hit trials (red) and miss trials (black), recorded from deep layers of target-aligned wMC ($n = 11$ sessions). ***D***, Hit trials, pooled across sessions from target-aligned wMC, grouped based on reaction time and aligned to the stimulus onset. Darker colors depict faster reaction time trials. Note the early "sensory" peak, invariant to reaction time. ***E***, Hit trials, pooled across sessions from target-aligned wMC, grouped based on reaction time (as in ***D***) and aligned to the reaction time. ***F–H***, Same as ***C–E*** but recorded from target-aligned DLS, also displaying robust sensory and motor alignments.

of trial outcome (Fig. 3*C*,*F*) and is time-locked to stimulus onset (within the first 100 ms) regardless of the reaction time (Fig. 3*D*, *G*). We do note differences in activity levels on hit vs miss trials (both prestimulus and poststimulus; Fig. 3*C*,*F*), which we analyze further below. To view preresponse activity, we aligned the spiking on each trial to the reaction time (Fig. 3*A*,*B*, right columns). Both twMC and tDLS displayed elevated activity before the response. However, preresponse ramping activity was more evident in tDLS than twMC. This can be better appreciated by clustering trials according to reaction time (Fig. 3*E*,*H*). This clustering demonstrates more pronounced transient activations in tDLS within 100 ms before the response regardless of the reaction time (Fig. 3*H*), potentially reflecting motor response triggering. Each of these qualitative

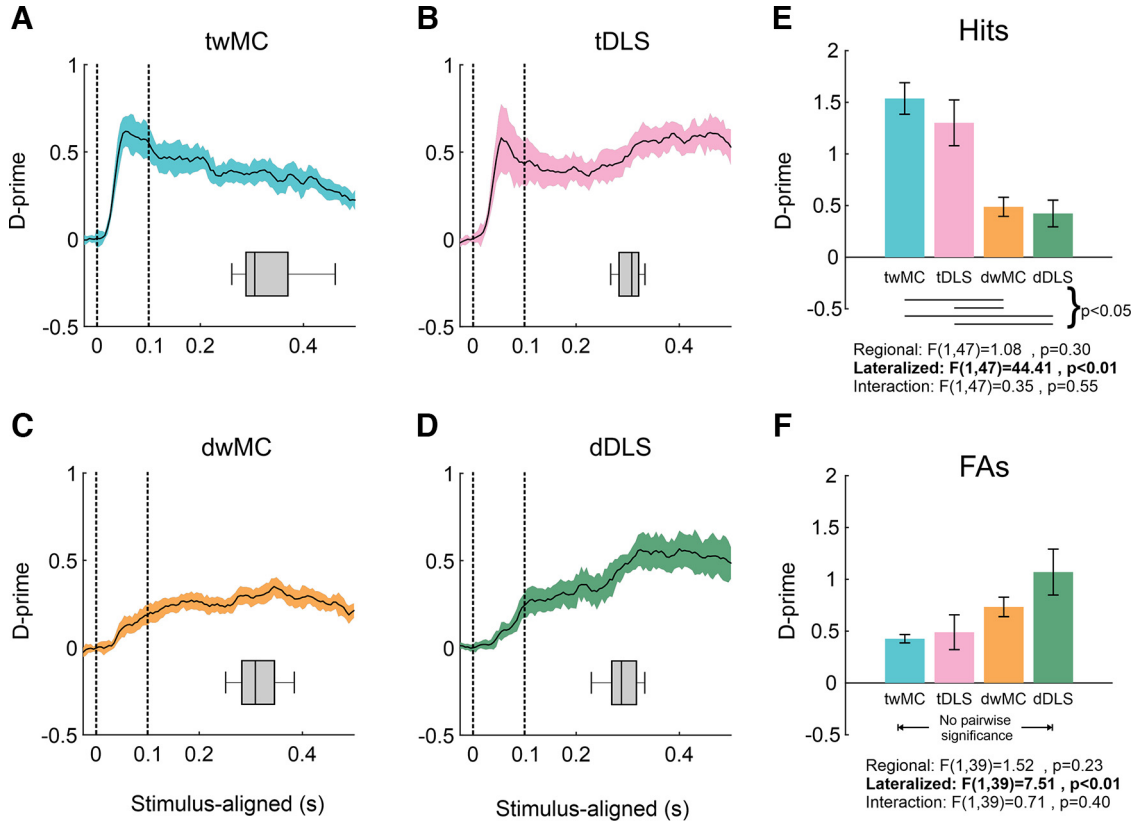

Figure 4. Lateralized sensory responses in wMC and DLS. ***A***, Average peak sensory encoding of target stimulus responses (hits) in deep layers of target-aligned wMC. The *x*-axis denotes time from stimulus onset in seconds. The *y*-axis denotes neurometric d-prime (as the separation between distributions of prestimulus and poststimulus MUA). Dashed lines indicate the 100-ms poststimulus window used for quantification in ***E***. The gray box-and-whisker plot indicates the reaction time distributions for the same recording sessions. ***B–D***, Same as ***A***, but for target-aligned DLS (***B***), distractor-aligned wMC (***C***), and distractor-aligned DLS (***D***). Note the rapid and large increase in d-prime after stimulus onset in target-aligned regions compared with distractor-aligned regions. ***E***, Sensory encoding of hit trials within each region calculated for the first 100 ms poststimulus across recording sessions. Lines under the bar graph indicate significant pairwise differences. ***F***, Same as ***E***, but for distractor stimulus responses (false alarms).

observations are followed up with quantitative analyses below (Figs. 4-6). However, they suggest that both wMC and DLS contain robust sensory-related and motor-related activity, with DLS more robustly signaling response triggering.

Lateralized sensory encoding in wMC and DLS

In the subsequent analyses, we present data from four brain regions: target-aligned wMC (twMC), target-aligned DLS (tDLS), distractor-aligned wMC (dwMC), and distractor-aligned DLS (dDLS). As such, our main quantification approach follows a 2×2 ANOVA design, assessing for main effects of region (wMC vs DLS) or hemisphere (target-aligned vs distractor-aligned).

To quantify sensory encoding in wMC and DLS, we computed the neurometric d-prime for each recording session (Fig. 4). We limited this analysis only to "response" trials (hits for target trials, false alarms for distractor trials), which presumably contain sensorimotor transformations. On hit trials, we observed that target-aligned regions (both twMC and tDLS) showed large, rapid-onset peaks in their neurometric d-prime profiles (Fig. 4*A*, *B*), compared with more slowly rising sensory encoding in distractor-aligned regions (Fig. 4*C*,*D*). Averaging across all recording sessions, sensory encoding for hit trials within the first 100 ms poststimulus (which is 100 ms before the earliest reaction times) peaked at (d-prime): twMC, 1.54 ± 0.15; tDLS, 1.30 ± 0.22; dwMC, 0.49 ± 0.09; dDLS, 0.42 ± 0.13 (Fig. 4*E*). From ANOVA testing, we observed a significant main effect of hemisphere (target-aligned vs distractor-aligned, $F_{(1,47)}$ = 44.41, p = 2.64E-8), no significant main effect of region (wMC vs DLS, $F_{(1,47)}$ = 1.08, p = 0.30), and no significant interaction ($F_{(1,47)}$ = 0.35, p = 0.55). Such findings indicate sensory encoding on hit trials that is lateralized and similar in twMC and tDLS.

We conducted similar sensory encoding analyses on false alarm trials (Fig. 4*F*). Again, the only statistically significant effect was of hemisphere (target-aligned vs distractor-aligned, $F_{(1,39)}$ = 7.51, p = 0.0092), yet with larger encoding in distractor-aligned regions. Together, these analyses demonstrate robust and lateralized sensory encoding in wMC and DLS, establishing potential functional contributions of both regions to sensory detection.

Preresponse peak firing and significant choice probability in wMC precedes DLS

Next, we sought to assess the latency of activation leading to response triggering. To accomplish this, we analyzed the time course of spiking activity in each region preceding reaction times on hit trials (Fig. 5). In all regions, we observed apparent ramping activity preceding reaction times (Fig. 5*A–D*). However, the time course of these ramping activations differed between regions. We quantified the delay between the 80th percentile of normalized peak neuronal activation and the reaction time (for twMC and tDLS example sessions see Fig. 5*E*). The activation-RT delay for each region was (seconds): twMC, 0.18 ± 0.01; tDLS, 0.11 ±0.02; dwMC, 0.13 ± 0.02; dDLS, 0.09 ± 0.02. Unlike analyses of sensory encoding, activation-RT delay ANOVA testing revealed a

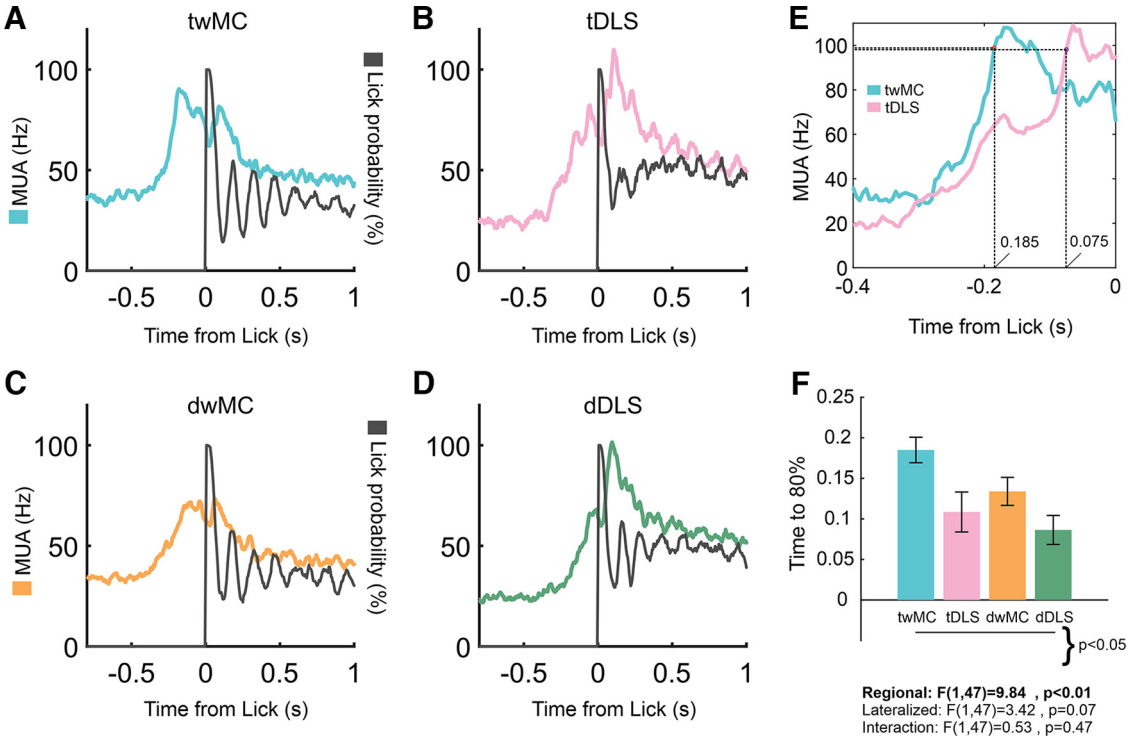

Figure 5. Preresponse peak firing in wMC precedes preresponse peak firing in DLS. ***A***, Average peak multiunit activity aligned to the lick responses on hit trials in deep layers of target-aligned wMC. The blue trace shows spike rate (Hz) whereas the black trace shows the lick probability (%). Note the increase in spiking activity before the licking response. ***B–D***, Same as ***A***, but for target-aligned DLS (***B***), distractor-aligned wMC (***C***), and distractor-aligned DLS (***D***). ***E***, Average peak multiunit activity for lick responses for example sessions from twMC and tDLS. Dashed lines show the 80th percentile of peak neuronal activation. ***F***, Delay between the 80th percentile of peak neuronal activation and reaction time across sessions for each recording site. Lines under the bar graph indicate significant pairwise differences.

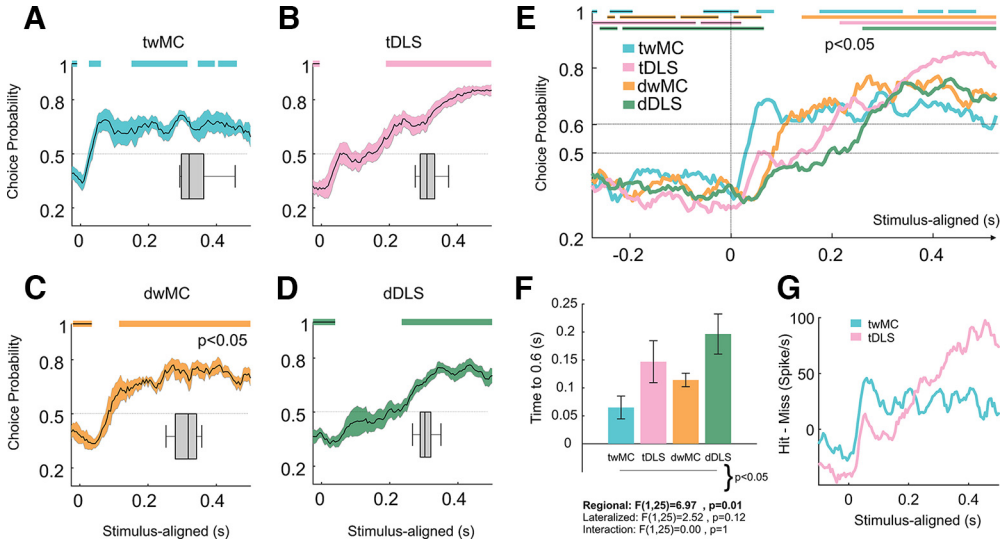

Figure 6. Choice probability in wMC precedes DLS. ***A***, Average choice probability on target trials in deep layers of target-aligned wMC. The *x*-axis denotes time from stimulus onset in seconds. The *y*-axis denotes choice probability calculated as the separation of spiking activity on hit and miss trials in 50-ms sliding windows with 90% overlap. Significant positive and negative choice probability time points are depicted by plain and filled color bars, respectively, at the top of the panel. Chance level (equal spiking on hit and miss trials) is depicted by the dashed line at 0.5. The gray box-and-whisker plot indicates the reaction time distributions for the same recording sessions. Note the early above chance choice probability, well preceding the reaction time. ***B–D***, Same as ***A***, but for target-aligned DLS (***B***), distractor-aligned wMC (***C***), and distractor-aligned DLS (***D***). ***E***, Choice probability traces, overlapped for all four regions, demonstrating differences in temporal profiles. In addition to chance (0.5), an arbitrary threshold at 0.6 is depicted by a dashed line. ***F***, Time to reach choice probability of 0.6 across sessions for each recording site. Lines under the bar graph indicate significant pairwise differences. ***G***, Differences in spike rates between the averages of hit trial and miss trials for twMC and tDLS. Both regions show initial increases immediately poststimulus. However, this increase is large and sustained for twMC, compared with a lower peak followed by a gradual increase into the response window for tDLS.

significant main effect of region (wMC vs DLS, $F_{(1,47)}$ = 9.84, p = 0.0029; Fig. 5*F*), with longer delays for wMC compared with DLS. We did not observe significant effects of hemisphere or interaction. To assess for the robustness of this effect we tested a range of spiking thresholds from 70% to 90%. Shorter latencies for DLS were found for all thresholds (main effect of region, wMC vs DLS, threshold of 70%: $F_{(1,47)}$ = 12.61, p = 0.0009, 75%: $F_{(1,47)}$ = 12.63, p = 0.0009, 80%: $F_{(1,47)}$ = 9.84, p = 0.0029, 85%: $F_{(1,47)}$ = 10.51,

$p = 0.0022$, 90%: $F_{(1,47)} = 7.57$, $p = 0.0084$). These analyses suggest that response triggering is more temporally aligned to the activation of DLS than wMC.

Next, we used choice probability analyses to gain insights into the temporal latencies of the sensorimotor transformations within each region (Fig. 6). Choice probability is the quantification of a relationship between neuronal activity and behavioral outcome, independent of stimulus amplitude (Britten et al., 1996). Above chance (0.5) choice probability indicates epochs in which neural activity is not solely accounted for by sensory processing and may instead reflect decision-making and/or motor response processing. In Figure 6*A–D*, we plot the choice probability time course for target stimuli, as the separation of spiking activity on hit versus miss trials. Target-aligned wMC shows prominent early choice probability peaks within 100 ms poststimulus (Fig. 6*A*). This finding in wMC is consistent with our previous report of early choice probability in layer 5 of wMC (Zareian et al., 2021). Distractor-aligned wMC shows moderate latency choice probability (Fig. 6*C*), whereas target-aligned and distractor-aligned DLS show more gradual rises in choice probability, peaking during the response window >200 ms poststimulus onset (Fig. 6*B*,*D*). A comparison of latencies to reach choice probability of 0.6 (Fig. 6*E*,*F*) revealed significantly earlier increases in wMC than DLS (seconds): twMC, 0.06 ± 0.02; tDLS, 0.15 ± 0.04; dwMC, 0.11 ± 0.01; dDLS, 0.20 ± 0.04; significant main effect of region (wMC vs DLS), $F_{(1,25)} = 6.97$, $p = 0.01$; no significant effect of hemisphere, $F_{(1,25)} = 2.52$, $p = 0.12$, or interaction, $F_{(1,25)} = 0$, $p = 1.00$. This earlier increase in choice probability in wMC can also be appreciated in the differences in average firing rates on hit versus miss trials for twMC compared with tDLS (Fig. 6*G*). Additionally, this finding of earlier choice probability in wMC than DLS was not reflective of differences in activity levels, as the effect was observed after matching spike rates across all four regions [latency to 0.6 choice probability, significant main effect of region (wMC vs DLS), $F_{(1,25)} = 4.97$, $p = 0.03$]. These analyses suggest that sensorimotor transformation signaling occurs earlier in wMC compared with DLS.

We recently reported lower than chance (negative) choice probability before stimulus onset throughout dorsal neocortex, indicating that lower prestimulus activity is more likely to result in response (vs no response) outcomes (Marrero et al., 2022). Interestingly, here we observed below chance prestimulus choice probability in both wMC and DLS (Fig. 6*A–E*). These prestimulus baseline differences can also be appreciated in plots of the average spike rates preceding hit and miss trials (Fig. 3*C*,*F*). Thus, noise suppression preceding whisker stimulus detection may generalize to cortical and subcortical structures.

In summary, we find robust sensory, motor, and choice-related signals in both wMC and DLS. Sensory signals are lateralized, whereas motor and choice signals are more regionally organized. Notably, we find a temporal differences of motor and choice signals between regions, with choice probability occurring earlier in wMC and response triggering more temporally aligned with activations of DLS.

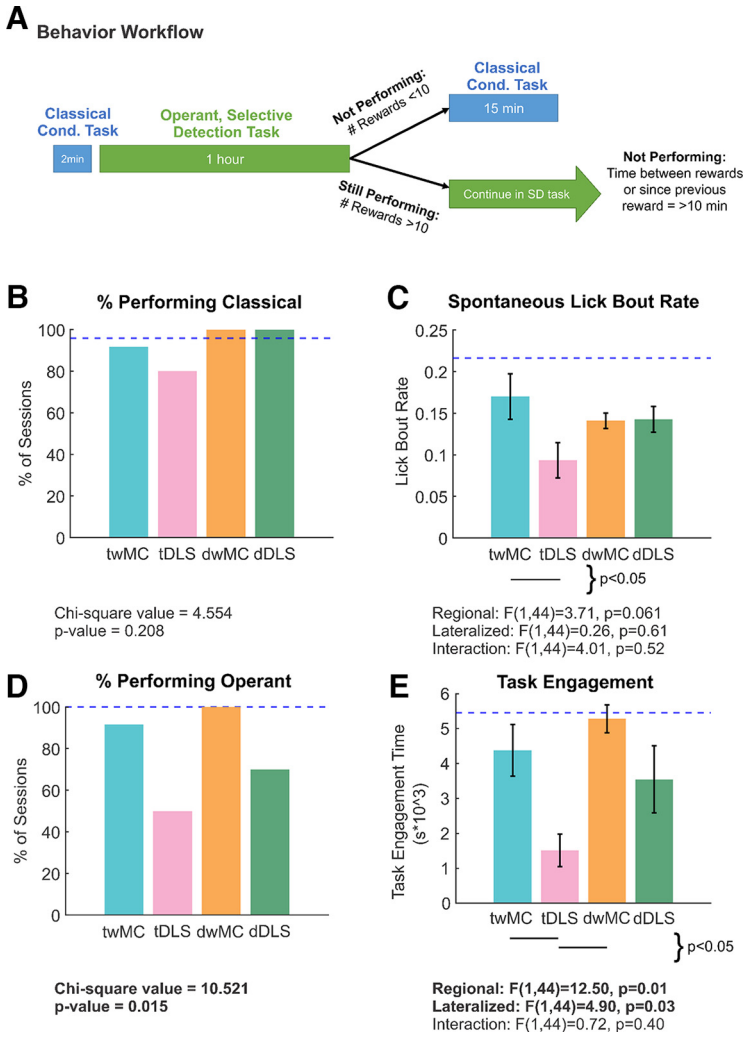

Figure 7. Muscimol inactivation impacts on task performance. ***A***, Behavioral training workflow for muscimol inactivation experiments (see also Materials and Methods). For each behavioral training session, mice were first presented with a classical conditioning task for 2 min, followed by the operant, selective detection task for 1 h. For mice that did not perform the selective detection task, they were again presented with the classical conditioning task for 15 min. Mice that did perform the selective detection task continued in this task until unmotivated. Panels ***B***, ***C*** refer to the classical conditioning task, panels ***D***, ***E*** refer to the operant, selective detection task. ***B***, Percentage of sessions meeting threshold performance for the classical conditioning task, according to region of inactivation. ***C***, Rate of spontaneous lick bouts during the classical conditioning task, averaged across all sessions according to the region of inactivation. ***D***, Percentage of sessions meeting threshold performance for the operant, selective detection task. ***E***, Duration of task engagement within the selective detection task, averaged across all sessions according to the region of inactivation. Lines under the bar graph indicate significant pairwise differences. For ***B–E***, the horizontal dashed line reflects performance measures from noninjected control sessions.

Task performance requires target-aligned DLS

Next, we performed muscimol ($GABA_A$ receptor agonist) inactivation studies to determine the essential functional contributions of wMC and DLS to task performance. Muscimol provides stable inactivation of the exposed region during behavioral testing, enabling assessment of its essential functions that cannot be compensated for on the order of minutes to hours (with full recovery of neural activity within 6 h; Arikan et al., 2002). In mice that had achieved expert performance, we alternated muscimol injected and control (noninjected) testing sessions, randomizing

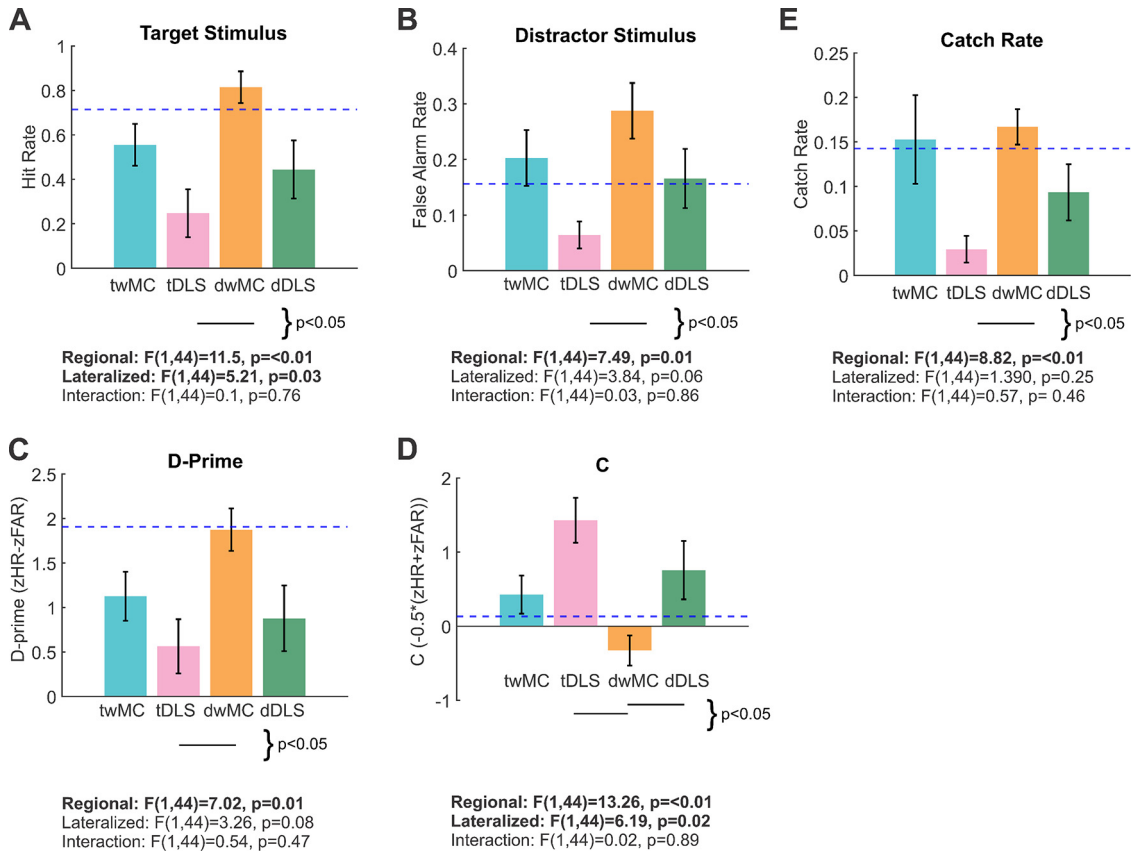

Figure 8. Target-aligned DLS inactivation reduces responding to task-related stimuli. ***A***, Hit rates within the selective detection task, averaged across all sessions according to the region of inactivation. Lines under the bar graph indicate significant pairwise differences. The horizontal dashed line reflects performance measures from noninjected control sessions. ***B–D***, Same as ***A***, but for false alarm rates (***B***), behavioral d-prime (***C***), criterion (***D***), and catch rate (***E***). Panels ***C***, ***D*** refer to the separation (d-prime) and response criterion (c) for stimulus discrimination, as computed from hit rates and false alarm rates. Note that target-aligned DLS inactivations (pink) caused large decreases in hit rates, false alarm rates, d-prime, catch rates, and corresponding increases in the criterion.

muscimol inactivations among the four sites (twMC, tDLS, dwMC, dDLS). (For localization and spread of injected fluorescent muscimol in control studies, see Fig. 2*D*,*H* and Materials and Methods.)

For each behavioral testing session (Fig. 7*A*), we first tested mice in a classical conditioning version of the task in which an auditory cue the mice had previously associated with reward (opening of a solenoid) was presented along with a fluid reward. This was performed to assess global deficiencies in motivation or response initiation/execution. In all inactivation conditions, mice performed this classical conditioning task at a high rate (Fig. 7*B*), with no significant differences between conditions (Pearson χ^2 value = 4.554, $p = 0.21$, threshold for "performing" as responding to >50% of rewards). Spontaneous licking during the classical conditioning task was lower for inactivation sessions (Fig. 7*C*). However, between regions of inactivation we did not observe main effects of region ($F_{(1,44)} = 3.71$, $p = 0.061$), hemisphere ($F_{(1,44)} = 0.26$, $p = 0.61$), or interaction ($F_{(1,44)} = 4.01$, $p = 0.052$), although spontaneous licking was significantly lower in tDLS than twMC ($p = 0.042$; Fig. 7*C*). These findings argue against severe global deficits in motivation or response execution.

In contrast, we did observe substantial group variance during subsequent performance in the operant, selective detection task (Fig. 7*D*; χ^2 value = 10.52, $p = 0.015$). Deficits in performance were particularly notable for target-aligned DLS inactivations, in which 50% of the behavioral sessions failed to attain a minimum number of rewards (<10 rewards within 1 h, compared with an average of 62 rewards for control mice, see also Materials and Methods for descriptions of performance thresholds). Additionally, we assessed task engagement time (Fig. 7*E*), quantified as the total time of engagement in the selective detection task (see Materials and Methods for assessment details). A two-way ANOVA test determined significant main effects of region ($F_{(1,44)} = 12.05$, $p = 0.0012$) and hemisphere ($F_{(1,44)} = 4.9$, $p = 0.033$), with target-aligned DLS inactivations displaying the greatest reductions in task engagement.

To better understand the contributions of each region to task performance, we assessed effects of inactivations on hit rate, false alarm rate, behavioral d-prime (separation between hit rate and false alarm rate), and criterion (tendency to respond on target and distractor trials) during the 1-h selective detection task (Fig. 8*A–D*). For all performance measures, we observed significant main effects of region (hit rate $p = 0.0016$; false alarm rate $p = 0.0091$; d-prime $p = 0.011$; criterion $p = 0.00080$), with additional main effects of hemisphere for hit rate and criterion ($p = 0.028$ and $p = 0.017$, respectively). Overall, DLS inactivations resulted in lower hit rates, lower false alarm rates, poorer target-distractor discrimination (d-prime), and reduced tendency to respond (c). For each measure, the largest impairments were observed for target-aligned DLS inactivations. Moreover, for each measure, target-aligned DLS inactivation sessions were significantly different from noninjected control sessions (task engagement time: control, 5460 ± 270 s; tDLS, 1510 ± 470 s, 72% reduction, $p = 8.19E-07$; hit rate: control, 0.71 ± 0.03; tDLS, 0.25 ± 0.11, 65% reduction, $p = 5.21E-06$; false alarm rate: control, 0.16 ± 0.01; tDLS: 0.06 ± 0.02, 63% reduction, $p = 1.93E-02$; d-prime:

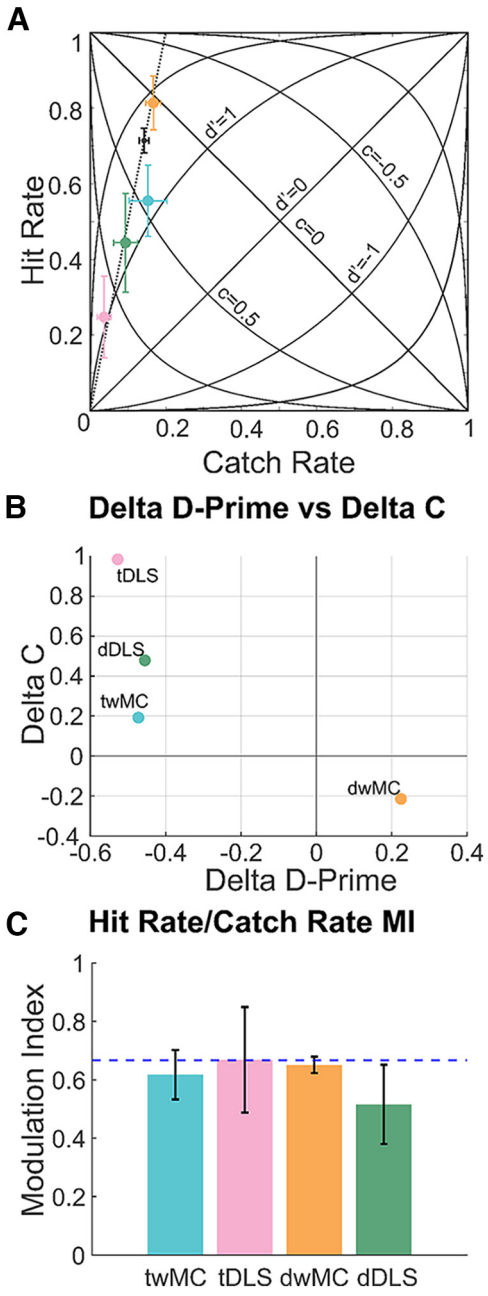

Figure 9. Inactivations differentially alter target stimulus sensory detection and response criterion but preserve hit rate to catch rate ratios. ***A***, Plots of hit rates (*y*-axis) and catch rates (*x*-axis) for control (black) and inactivation sessions. Overlaid on this plot are three reference dimensions. Sensory detection (d-prime) and response criterion (c) manifolds are plotted for different values. Also included is a dotted line through the origin and control data, reflecting proportional changes in hit rate and catch rate. Note the alignment of the inactivation data to the proportion line. ***B***, Scatter plot of average changes in target detection (*x*-axis, Δ d-prime) and response criterion (*y*-axis, Δ c) for inactivation sessions compared with control sessions. wMC inactivations caused bidirectional changes in both measures, whereas DLS inactivations were unidirectional with increasing effects on response criterion. ***C***, Modulation indices of hit rate to catch rate, demonstrating constant proportions across experimental conditions.

control, 1.91 ± 0.11; tDLS, 0.56 ± 0.31, 71% reduction, $p = 7.87E\text{-}05$; criterion: control, 0.13 ± 0.08; tDLS, 1.43 ± 0.30, 11-fold increase, $p = 1.03E\text{-}06$). These data identify target-aligned DLS, rather than wMC, as most critical for responding to task-related stimuli.

Interestingly, we found that muscimol inactivation did not invariably reduce response rates. Inactivations of wMC resulted in increased false alarm rates compared with control sessions (Fig. 8*B*), which was statistically significant for distractor-aligned wMC inactivations (control, 0.16 ± 0.03; dwMC, 0.29 ± 0.05, 81% increase $p = 0.0010$). For multiple measures, effects of target-aligned DLS inactivation versus distractor-aligned wMC inactivation were significantly different from each other and opposite in direction compared with control sessions. This includes hit rate (tDLS, 0.25 ± 0.11; dwMC: 0.82 ± 0.07, $p = 0.0012$), false alarm rate (tDLS, 0.06 ±0.02; dwMC, 0.29±0.05, $p = 0.0091$), criterion (c; tDLS, 1.43 ± 0.30; dwMC, −0.33 ± 0.20, $p = 0.00046$), and catch rate (tDLS, 0.029 ± 0.015; dwMC, 0.17 ± 0.020, $p = 0.025$). These findings highlight the divergent functional contributions of these two regions on task performance, with target-aligned DLS dominantly contributing to sensory selection and distractor-aligned wMC dominantly contributing to distractor response suppression.

To assess motivation/impulsivity as a driver of the observed behavioral effects, first we analyzed catch rates during the operant, selective detection task as a measure of the stimulus-independent tendency to respond (Fig. 8*E*). We observed a significant main effect of region ($p = 0.005$), with significantly lower catch rates for DLS than wMC, and a particularly large reduction for tDLS.

How much of the changes in target stimulus hit rates can be accounted for by changes in the tendency to respond? In a signal detection theory framework, changes in the tendency to respond (quantified as the criterion, c) can be distinguished from sensory detection (quantified as d-prime). Therefore, we replotted hit and catch rates on d-prime and c contour lines (Fig. 9*A*). Changes in sensory detection that do not alter the tendency to respond occur along the same c manifold; changes in the tendency to respond that do not alter sensory detection occur along the d-prime manifold. Notably, the inactivation data differ from control data in both d-prime and c dimensions, indicating changes in both sensory detection and the tendency to respond. We summarize these differences in Figure 9*B* as the changes from control sessions for each region of inactivation. We note that twMC and dwMC had opposite effects on both d-prime and c, with twMC decreasing both sensory detection (decrease in d-prime) and the tendency to respond (increase in c). DLS inactivations caused similar reductions in sensory detection (decreases in d-prime) as twMC, but with larger reductions in the tendency to respond (increases in c), with the largest changes in c from tDLS inactivations.

Interestingly, we note a different dimension that appears to account for the hit and catch rate changes; that is, the proportion of hit rate to catch rate (note the linear relationship between hit rate and catch rate in Fig. 9*A*). In Figure 9*C*, we plot the modulation indices for hit rate versus catch rate [(HR − CR)/(HR + CR)]. This proportion is not different across regions of inactivation, and not different from control sessions. Overall, we conclude that these inactivations had various effects on sensory detection and response criterion, yet in a way that maintains the proportion of hit rate to catch rate (with the largest reductions in both from tDLS inactivations).

Discussion

In this study, we compared whisker motor cortex (wMC) and dorsolateral striatum (DLS) contributions to performance in a learned selective detection task. First, we identified the S1-projection sites within wMC and DLS as our target regions (Fig. 2). Next, we demonstrated that during expert task performance,

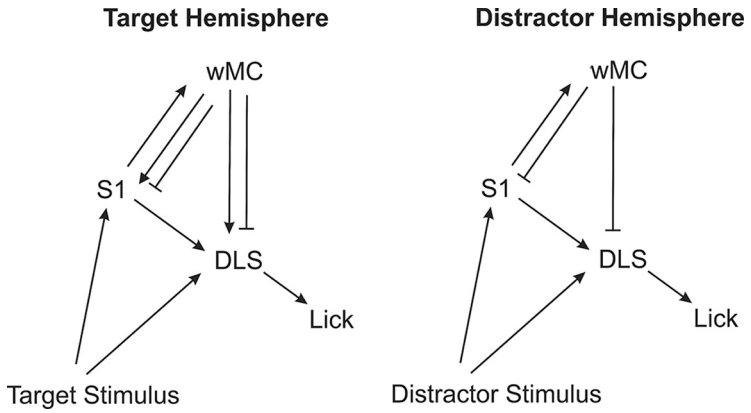

Figure 10. Functional circuit model for how wMC and DLS interact to implement sensorimotor transformations. Arrows depict net excitatory pathways whereas blunt arrows depict net inhibitory pathways. In this model, target-aligned DLS functions as a critical node in transforming sensory inputs into motor outputs, potentially integrating sensory evidence from S1, wMC, and subcortical regions. In contrast, wMC acts primarily to modulate the sensorimotor transformations that occur through the DLS pathway. While not depicted here, our data support bilateral contributions of DLS to response triggering for both stimuli, with an overall greater involvement of target-aligned DLS.

both regions display robust sensory encoding (Figs. 3, 4) as well as motor-related and choice-related signals (Figs. 3, 5, 6). Lastly, targeted pharmacological inactivation studies identified DLS as essential for responding to task-related stimuli, in contrast to bidirectional modulatory contributions of wMC (Figs. 7-9). Collectively, our data support DLS as a crucial bottleneck in linking task-related stimuli to prepotent responses in this learned task (Fig. 10).

One important consideration when interpreting inactivation studies, particularly for Go/NoGo tasks, is that reductions in task performance may reflect global deficits in motivation, sensation, or response execution rather than specific deficits in task-related processing (Carandini and Churchland, 2013). We interpret the robust impairments during DLS inactivation as reflecting specific deficits in task-related processing for multiple reasons. Most importantly, during the same behavioral sessions, mice with DLS inactivations responded at high rates to auditory-cued reward delivery (Fig. 7*B*), ruling out severe global deficits. Additionally, we observed robust poststimulus (sensory) and preresponse (possibly motor command) signals within DLS, as would be required for participation in sensorimotor transformations. Whether the actual sensorimotor transformation is computed within DLS or is computed elsewhere and propagated to DLS remains unknown. However, our data support DLS as an indispensable node in the sensorimotor transformation process in this task.

Our findings support current frameworks for the importance of DLS in learned tasks (Atallah et al., 2007; Dhawale et al., 2021). An unexpected finding is that target-aligned DLS inactivations did not only reduce responding to target stimuli (Fig. 8*A*), but also robustly reduced responding to distractor stimuli (Fig. 8*B*). We speculate that through learning, response triggering for target and distractor stimuli become conditioned on the activation of target-aligned DLS. Understanding the neural mechanisms underlying this conditioned response triggering, and its possible dependence on dopamine neuromodulation (Gerfen et al., 1990; Surmeier et al., 1996; Kravitz et al., 2010; Gerfen and Surmeier, 2011) are important topics of future research. Relatedly, we were surprised to find that distractor-aligned DLS inactivations caused robust behavioral deficits, particularly in reducing target stimulus hit rates (Fig. 8*A*). We believe that this is due to the bilateral response (straight-forward lick) required for reporting detection, and the known projections (both direct and indirect) from unilateral S1 to bilateral DLS (e.g. Reig and Silberberg, 2016). One of the features of this behavioral task is that the mice must convert a unilateral sensory input into a bilateral motor response. We would expect early sensory regions (e.g., VPM thalamus) to make purely unilateral contributions, and late motor regions (e.g., hypoglossal nucleus) to make symmetric bilateral contributions. That DLS shows an intermediate profile (bilateral contributions yet biased to target-aligned) suggests that it is participating at an intermediate stage within the sensorimotor transformation.

It was recently proposed that baseline (prestimulus) activity within the striatum may regulate task engagement, with higher prestimulus activity priming motor execution by bringing the network closer to response threshold (Steinmetz et al., 2019). This framework would have predicted above chance prestimulus choice probability for target-aligned DLS. In contrast, we find that bilateral DLS, like the rest of dorsal neocortex (Marrero et al., 2022), displays below chance prestimulus choice probability in response to target stimuli (Fig. 6*E*). This difference may be due to sensory modality or task design. In particular, detection of a transient whisker deflection is reduced when subjects are whisking during stimulus delivery (Ollerenshaw et al., 2012; Kyriakatos et al., 2017; Marrero et al., 2022). Therefore, a low activity prestimulus state (both neural and behavioral) may be optimal for detection of small amplitude whisker stimuli (Marrero et al., 2022).

An important open question is which basal ganglia outputs are most relevant for response triggering. The basal ganglia may project back to regions of motor/frontal cortex not studied here which may ultimately signal the motor command. Possibilities include tongue-jaw motor cortex (Mayrhofer et al., 2019) and anterior lateral motor cortex (Guo et al., 2014; Li et al., 2015), two frontal cortices involved in the execution and planning of goal-directed licking. And yet, there is growing appreciation of direct projections from the basal ganglia to subcortical motor structures, including the superior colliculus and other brainstem motor structures (Saitoh et al., 2003; Takakusaki et al., 2003, 2011; J. Lee and Sabatini, 2021). We speculate that, at least in the rodent, striatal selection does not require motor cortex for response execution.

In comparison to the DLS, the functional contributions of wMC were more nuanced. Inactivations of wMC caused increases or decreased in response rates, depending on the stimulus identity and target versus distractor alignment. Recent studies have shown that motor cortex is required for skill learning, yet is dispensable for performing well-learned tasks (Kawai et al., 2015; Hwang et al., 2021). Thus, it is possible that sensorimotor processing through wMC is more important during learning than during expert performance as tested in this study. Yet, in the expert mouse, we find that wMC functions in a modulatory role to increase or decrease sensory detection and response criterion. This was particularly notable for distractor stimuli, for which wMC inactivations increased false alarm rates compared with control sessions (Fig. 8*B*). This finding is consistent with a growing literature, primarily in rodents, suggesting essential roles of motor cortices in

suppressing prepotent responses (Zagha et al., 2015; Ebbesen and Brecht, 2017; Murakami et al., 2017). Moreover, given the similarities in representation yet distinct functions of wMC and DLS, this study emphasizes the limitations of inferring causal contributions from recording studies alone.

Despite the different functional effects of wMC and DLS inactivations, we noted that each region altered sensory detection and response criterion in a manner that preserved the proportion of hit rate to catch rate. We can only speculate as to the meaning of this consistent relationship. Subjects can independently change their sensory detection or response criterion according to reward structure (Luo and Maunsell, 2018), and therefore these combined effects do not reflect an obligatory behavioral compensation or artifact of signal detection theory. One possible explanation is that wMC and DLS directly contribute to both sensory response gain and decision threshold. An alternative possibility is that wMC and DLS exclusively contribute to sensory response gain, and that downstream decision-making regions adjust their decision threshold to maintain a stable reward efficiency. Future perturbation experiments, while recording from downstream decision-making regions, are needed to distinguish between these possibilities.

We do recognize important limitations of our study. Foremost, the multiunit activities analyzed here represent the summed spiking outputs of neuronal ensembles consisting of different cell-types. While we do observe systematic differences in the dynamics of preresponse and choice-related signals in wMC and DLS, we recognize that there is likely a much larger heterogeneity of responses of single units. Second, our pharmacological inactivations do not distinguish between the multiple output pathways that may be responsible for the consequent behavioral effects. Follow-up studies with cell-type resolution and pathway-specificity will provide many important mechanistic insights into how DLS and wMC contribute to sensorimotor transformations.

Our findings are generally consistent with previous studies of wMC in whisker detection tasks. Recently, Esmaeili et al. (2021) demonstrated modest reductions in hit rates and increases in false alarm rates when inactivating stimulus-aligned whisker motor cortex during whisker stimulation (Esmaeili et al., 2021). Similar, yet nonstatistically significant, trends were observed in (Le Merre et al., 2018). These findings contrast with large reductions in hit rates due to inactivations of S1 and secondary somatosensory cortex (S2) during whisker stimulation, or secondary whisker motor cortex and tongue-jaw motor cortex during the response window (Le Merre et al., 2018; Esmaeili et al., 2021). Understanding the signaling between these regions and the DLS will likely be key to developing a mechanistic framework of sensorimotor transformations in whisker detection tasks (see also (Chen et al., 2013; Sippy et al., 2015; Kwon et al., 2016; Yamashita and Petersen, 2016; Yang et al., 2016).

References

Alexander GE, Crutcher MD (1990) Functional architecture of basal ganglia circuits: neural substrates of parallel processing. Trends Neurosci 13:266–271.

Allen Institute for Brain Science (2004) Allen Mouse Brain Atlas [Connectivity Atlas]. Available at https://mouse.brain-map.org/.

Antzoulatos EG, Miller EK (2011) Differences between neural activity in prefrontal cortex and striatum during learning of novel abstract categories. Neuron 71:243–249.

Arikan R, Blake NMJ, Erinjeri JP, Woolsey TA, Giraud L, Highstein SM (2002) A method to measure the effective spread of focally injected muscimol into the central nervous system with electrophysiology and light microscopy. J Neurosci Methods 118:51–57.

Aruljothi K, Marrero K, Zhang Z, Zareian B, Zagha E (2020) Functional localization of an attenuating filter within cortex for a selective detection task in mice. J Neurosci 40:5443–5454.

Atallah HE, Lopez-Paniagua D, Rudy JW, O'Reilly RC (2007) Separate neural substrates for skill learning and performance in the ventral and dorsal striatum. Nat Neurosci 10:126–131.

Bergstrom HC, Lipkin AM, Lieberman AG, Pinard CR, Gunduz-Cinar O, Brockway ET, Taylor WW, Nonaka M, Bukalo O, Wills TA, Rubio FJ, Li X, Pickens CL, Winder DG, Holmes A (2018) Dorsolateral striatum engagement interferes with early discrimination learning. Cell Rep 23:2264–2272.

Bergstrom HC, Lieberman AG, Graybeal C, Lipkin AM, Holmes A (2020) Dorsolateral striatum engagement during reversal learning. Learn Mem 27:418–422.

Britten KH, Newsome WT, Shadlen MN, Celebrini S, Movshon JA (1996) A relationship between behavioral choice and the visual responses of neurons in macaque MT. Vis Neurosci 13:87–100.

Brockett AT, Tennyson SS, deBettencourt CA, Kallmyer M, Roesch MR (2022) Medial prefrontal cortex lesions disrupt prepotent action selection signals in dorsomedial striatum. Curr Biol 32:3276–3287.e3.

Carandini M, Churchland AK (2013) Probing perceptual decisions in rodents. Nat Neurosci 16:824–831.

Chen JL, Carta S, Soldado-Magraner J, Schneider BL, Helmchen F (2013) Behaviour-dependent recruitment of long-range projection neurons in somatosensory cortex. Nature 499:336–340.

Clarke HF, Robbins TW, Roberts AC (2008) Lesions of the medial striatum in monkeys produce perseverative impairments during reversal learning similar to those produced by lesions of the orbitofrontal cortex. J Neurosci 28:10972–10982.

de Lafuente V, Romo R (2006) Neural correlate of subjective sensory experience gradually builds up across cortical areas. Proc Natl Acad Sci U S A 103:14266–14271.

Dhawale AK, Wolff SBE, Ko R, Ölveczky BP (2021) The basal ganglia control the detailed kinematics of learned motor skills. Nat Neurosci 24:1256–1269.

Ebbesen CL, Brecht M (2017) Motor cortex—to act or not to act? Nat Rev Neurosci 18:694–705.

Esmaeili V, Tamura K, Muscinelli SP, Modirshanechi A, Boscaglia M, Lee AB, Oryshchuk A, Foustoukos G, Liu Y, Crochet S, Gerstner W, Petersen CCH (2021) Rapid suppression and sustained activation of distinct cortical regions for a delayed sensory-triggered motor response. Neuron 109:2183–2201.e9.

Finkelstein A, Fontolan L, Economo MN, Li N, Romani S, Svoboda K (2021) Attractor dynamics gate cortical information flow during decision-making. Nat Neurosci 24:843–850.

Foster NN, et al. (2021) The mouse cortico–basal ganglia–thalamic network. Nature 598:188–194.

Frank MJ, Loughry B, O'Reilly RC (2001) Interactions between frontal cortex and basal ganglia in working memory: a computational model. Cogn Affect Behav Neurosci 1:137–160.

Gerfen CR, Surmeier DJ (2011) Modulation of striatal projection systems by dopamine. Annu Rev Neurosci 34:441–466.

Gerfen CR, Engber TM, Mahan LC, Susel Z, Chase TN, Monsma FJ Jr, Sibley DR (1990) D1 and D2 dopamine receptor-regulated gene expression of striatonigral and striatopallidal neurons. Science 250:1429–1432.

Gordon EM, Laumann TO, Marek S, Newbold DJ, Hampton JM, Seider NA, Montez DF, Nielsen AM, Van AN, Zheng A, Miller R, Siegel JS, Kay BP, Snyder AZ, Greene DJ, Schlaggar BL, Petersen SE, Nelson SM, Dosenbach NUF (2022) Individualized functional subnetworks connect human striatum and frontal cortex. Cereb Cortex 32:2868–2884.

Graybiel AM, Aosaki T, Flaherty AW, Kimura M (1994) The basal ganglia and adaptive motor control. Science 265:1826–1831.

Grillner S, Hellgren J, Ménard A, Saitoh K, Wikström MA (2005) Mechanisms for selection of basic motor programs–roles for the striatum and pallidum. Trends Neurosci 28:364–370.

Guo ZV, Li N, Huber D, Ophir E, Gutnisky D, Ting JT, Feng G, Svoboda K (2014) Flow of cortical activity underlying a tactile decision in mice. Neuron 81:179–194.

Guo ZV, Inagaki HK, Daie K, Druckmann S, Gerfen CR, Svoboda K (2017) Maintenance of persistent activity in a frontal thalamocortical loop. Nature 545:181–186.

Hanes DP, Schall JD (1996) Neural control of voluntary movement initiation. Science 274:427–430.

Hintiryan H, Foster NN, Bowman I, Bay M, Song MY, Gou L, Yamashita S, Bienkowski MS, Zingg B, Zhu M, Yang XW, Shih JC, Toga AW, Dong H-W (2016) The mouse cortico-striatal projectome. Nat Neurosci 19:1100–1114.

Hong YK, Lacefield CO, Rodgers CC, Bruno RM (2018) Sensation, movement and learning in the absence of barrel cortex. Nature 561:542–546.
Hooks BM, Mao T, Gutnisky DA, Yamawaki N, Svoboda K, Shepherd GM (2013) Organization of cortical and thalamic input to pyramidal neurons in mouse motor cortex. J Neurosci 33:748–760.
Hoover JE, Strick PL (1999) The organization of cerebellar and basal ganglia outputs to primary motor cortex as revealed by retrograde transneuronal transport of herpes simplex virus type 1. J Neurosci 19:1446–1463.
Hunnicutt BJ, Jongbloets BC, Birdsong WT, Gertz KJ, Zhong H, Mao T (2016) A comprehensive excitatory input map of the striatum reveals novel functional organization. Elife 5:e19103.
Hwang EJ, Dahlen JE, Mukundan M, Komiyama T (2021) Disengagement of motor cortex during long-term learning tracks the performance level of learned movements. J Neurosci 41:7029–7047.
Inagaki HK, Fontolan L, Romani S, Svoboda K (2019) Discrete attractor dynamics underlies persistent activity in the frontal cortex. Nature 566:212–217.
Jin X, Costa RM (2010) Start/stop signals emerge in nigrostriatal circuits during sequence learning. Nature 466:457–462.
Kawai R, Markman T, Poddar R, Ko R, Fantana AL, Dhawale AK, Kampff AR, Ölveczky BP (2015) Motor cortex is required for learning but not for executing a motor skill. Neuron 86:800–812.
Kravitz AV, Freeze BS, Parker PR, Kay K, Thwin MT, Deisseroth K, Kreitzer AC (2010) Regulation of parkinsonian motor behaviours by optogenetic control of basal ganglia circuitry. Nature 466:622–626.
Kupferschmidt DA, Juczewski K, Cui G, Johnson KA, Lovinger DM (2017) Parallel, but dissociable, processing in discrete corticostriatal inputs encodes skill learning. Neuron 96:476–489.e5.
Kwon SE, Yang H, Minamisawa G, O'Connor DH (2016) Sensory and decision-related activity propagate in a cortical feedback loop during touch perception. Nat Neurosci 19:1243–1249.
Kyriakatos A, Sadashivaiah V, Zhang Y, Motta A, Auffret M, Petersen CC (2017) Voltage-sensitive dye imaging of mouse neocortex during a whisker detection task. Neurophotonics 4:031204.
Le Merre P, Esmaeili V, Charrière E, Galan K, Salin PA, Petersen CCH, Crochet S (2018) Reward-based learning drives rapid sensory signals in medial prefrontal cortex and dorsal hippocampus necessary for goal-directed behavior. Neuron 97:83–91.e5.
Lee CR, Yonk AJ, Wiskerke J, Paradiso KG, Tepper JM, Margolis DJ (2019) Opposing influence of sensory and motor cortical input on striatal circuitry and choice behavior. Curr Biol 29:1313–1323.e5.
Lee J, Sabatini BL (2021) Striatal indirect pathway mediates exploration via collicular competition. Nature 599:645–649.
Li N, Chen TW, Guo ZV, Gerfen CR, Svoboda K (2015) A motor cortex circuit for motor planning and movement. Nature 519:51–56.
Li N, Daie K, Svoboda K, Druckmann S (2016) Robust neuronal dynamics in premotor cortex during motor planning. Nature 532:459–464.
Luo TZ, Maunsell JHR (2018) Attentional changes in either criterion or sensitivity are associated with robust modulations in lateral prefrontal cortex. Neuron 97:1382–1393.e7.
Mao T, Kusefoglu D, Hooks Bryan M, Huber D, Petreanu L, Svoboda K (2011) Long-range neuronal circuits underlying the interaction between sensory and motor cortex. Neuron 72:111–123.
Marrero K, Aruljothi K, Zareian B, Gao C, Zhang Z, Zagha E (2022) Global, low-amplitude cortical state predicts response outcomes in a selective detection task in mice. Cereb Cortex 32:2037–2053.
Mayrhofer JM, El-Boustani S, Foustoukos G, Auffret M, Tamura K, Petersen CCH (2019) Distinct contributions of whisker sensory cortex and tongue-jaw motor cortex in a goal-directed sensorimotor transformation. Neuron 103:1034–1043.e5.
McGeorge A, Faull R (1987) The organization and collateralization of corticostriate neurones in the motor and sensory cortex of the rat brain. Brain Res 423:318–324.
Middleton FA, Strick PL (2000) Basal ganglia output and cognition: evidence from anatomical, behavioral, and clinical studies. Brain Cogn 42:183–200.
Mink JW (1996) The basal ganglia: focused selection and inhibition of competing motor programs. Prog Neurobiol 50:381–425.
Moran J, Desimone R (1985) Selective attention gates visual processing in the extrastriate cortex. Science 229:782–784.
Muhammad R, Wallis JD, Miller EK (2006) A comparison of abstract rules in the prefrontal cortex, premotor cortex, inferior temporal cortex, and striatum. J Cogn Neurosci 18:974–989.
Murakami M, Shteingart H, Loewenstein Y, Mainen ZF (2017) Distinct sources of deterministic and stochastic components of action timing decisions in rodent frontal cortex. Neuron 94:908–919.e7.
Oh SW, et al. (2014) A mesoscale connectome of the mouse brain. Nature 508:207–214.
Ollerenshaw DR, Bari BA, Millard DC, Orr LE, Wang Q, Stanley GB (2012) Detection of tactile inputs in the rat vibrissa pathway. J Neurophysiol 108:479–490.
Pasupathy A, Miller EK (2005) Different time courses of learning-related activity in the prefrontal cortex and striatum. Nature 433:873–876.
Paxinos G, Franklin KB (2019) Paxinos and Franklin's the mouse brain in stereotaxic coordinates. San Diego: Academic Press.
Peters AJ, Fabre JM, Steinmetz NA, Harris KD, Carandini M (2021) Striatal activity topographically reflects cortical activity. Nature 591:420–425.
Pimentel-Farfan AK, Báez-Cordero AS, Peña-Rangel TM, Rueda-Orozco PE (2022) Cortico-striatal circuits for bilaterally coordinated movements. Sci Adv 8:eabk2241.
Redgrave P, Prescott TJ, Gurney K (1999) The basal ganglia: a vertebrate solution to the selection problem? Neuroscience 89:1009–1023.
Reig R, Silberberg G (2016) Distinct corticostriatal and intracortical pathways mediate bilateral sensory responses in the striatum. Cereb Cortex 26:4405–4415.
Saitoh K, Hattori S, Song WJ, Isa T, Takakusaki K (2003) Nigral GABAergic inhibition upon cholinergic neurons in the rat pedunculopontine tegmental nucleus. Eur J Neurosci 18:879–886.
Salinas E, Romo R (1998) Conversion of sensory signals into motor commands in primary motor cortex. J Neurosci 18:499–511.
Salkoff DB, Zagha E, McCarthy E, McCormick DA (2020) Movement and performance explain widespread cortical activity in a visual detection task. Cereb Cortex 30:421–437.
Saunders A, Oldenburg IA, Berezovskii VK, Johnson CA, Kingery ND, Elliott HL, Xie T, Gerfen CR, Sabatini BL (2015) A direct GABAergic output from the basal ganglia to frontal cortex. Nature 521:85–89.
Siegel M, Buschman TJ, Miller EK (2015) Cortical information flow during flexible sensorimotor decisions. Science 348:1352–1355.
Sippy T, Lapray D, Crochet S, Petersen CC (2015) Cell-type-specific sensorimotor processing in striatal projection neurons during goal-directed behavior. Neuron 88:298–305.
Steinmetz NA, Zatka-Haas P, Carandini M, Harris KD (2019) Distributed coding of choice, action and engagement across the mouse brain. Nature 576:266–273.
Stephenson-Jones M, Samuelsson E, Ericsson J, Robertson B, Grillner S (2011) Evolutionary conservation of the basal ganglia as a common vertebrate mechanism for action selection. Curr Biol 21:1081–1091.
Surmeier DJ, Song WJ, Yan Z (1996) Coordinated expression of dopamine receptors in neostriatal medium spiny neurons. J Neurosci 16:6579–6591.
Takakusaki K, Habaguchi T, Ohtinata-Sugimoto J, Saitoh K, Sakamoto T (2003) Basal ganglia efferents to the brainstem centers controlling postural muscle tone and locomotion: a new concept for understanding motor disorders in basal ganglia dysfunction. Neuroscience 119:293–308.
Takakusaki K, Obara K, Nozu T, Okumura T (2011) Modulatory effects of the GABAergic basal ganglia neurons on the PPN and the muscle tone inhibitory system in cats. Arch Ital Biol 149:385–405.
Utter AA, Basso MA (2008) The basal ganglia: an overview of circuits and function. Neurosci Biobehav Rev 32:333–342.
Yamashita T, Petersen C (2016) Target-specific membrane potential dynamics of neocortical projection neurons during goal-directed behavior. Elife 5:e15798.
Yang H, Kwon SE, Severson KS, O'Connor DH (2016) Origins of choice-related activity in mouse somatosensory cortex. Nat Neurosci 19:127–134.
Yin HH, Knowlton BJ (2006) The role of the basal ganglia in habit formation. Nat Rev Neurosci 7:464–476.
Yin HH, Knowlton BJ, Balleine BW (2004) Lesions of dorsolateral striatum preserve outcome expectancy but disrupt habit formation in instrumental learning. Eur J Neurosci 19:181–189.
Zagha E, Ge X, McCormick DA (2015) Competing neural ensembles in motor cortex gate goal-directed motor output. Neuron 88:565–577.
Zareian B, Zhang Z, Zagha E (2021) Cortical localization of the sensory-motor transformation in a whisker detection task in mice. eNeuro 8: ENEURO.0004-21.2021.